J Vis
https://doi.org/10.1007/s12650-022-00827-w

REGULAR PAPER

Ryota Fukunaga · Masatoshi Ezoe · Shinichiro Nakao · Yoshiaki Miyazato

Application of rainbow schlieren tomography for shock-containing rectangular jets

Received: 25 March 2021 / Revised: 16 December 2021 / Accepted: 18 January 2022

Abstract The shock-containing jet issued from a rectangular convergent nozzle with an aspect ratio of 4.0 at the exit is captured quantitatively by the rainbow schlieren tomography. Multiple viewing rainbow schlieren pictures of the jet are taken for a nozzle pressure ratio of 4.0 to produce a strong shock with a Mach stem in the jet plume. The convolution back-projection (CBP) method is utilized to reconstruct the three-dimensional density field of the jet. The flow topology of an intricate near-field shock system in the jet is displayed vividly by a bird's eye view representation of the isopycnic field with a high spatial resolution

Keywords Rainbow schlieren · Computed tomography · Supersonic jet · Rectangular nozzle · Shock wave

1 Introduction

Rectangular supersonic jets attract special attentions because of their enhanced mixing for combustion applications and high-speed jet noise suppression compared to those of comparable axisymmetric supersonic jets. The ability to promote supersonic flow mixing and reduce noise from supersonic jets is strongly affected by the jet structure. The quantitative information of the velocity, density, and temperature in the flow field is required to understand the jet characteristics. However, non-intrusive quantitative measurements in the near-field region of supersonic rectangular jets with strong shocks such as the Mach stem and intercepting shock are virtually non-existent because of the formidable challenge even now.

Krothapalli et al. (1986) utilized a conventional schlieren method along with hot-wire measurements in the jet to study the mean and turbulent velocity fields of an underexpanded rectangular jet of moderate aspect ratio. Gutmark et al. (1990) studied experimentally underexpanded sonic jets from circular, rectangular, and elliptic nozzles by a schlieren technique to visualize both of the shock structure and the small-scale turbulence in the different planes of the noncircular nozzle configurations. In addition, hot-wire anemometry was used to determine the spreading rate of the jet, and near-field pressure fluctuations measurements were carried out to investigate the shook-cell and shear-layer structure variation with the nozzle pressure ratio. Raman and Rice (1994) used a focusing schlieren system with steady light for continuous monitoring of the jet during the measurements to investigate hydrodynamic instability modes excited by screech tones from a rectangular underexpanded jet. Alkislar et al. (2003) applied stereoscopic particle image velocimetry (PIV) for a screeching rectangular jet to investigate the three-dimensional flow

R. Fukunaga · S. Nakao · Y. Miyazato (✉)
Department of Mechanical Systems Engineering, The University of Kitakyushu, 1-1 Hibikino, Wakamatsu-ku, Kitakyushu 808-0135, Japan
E-mail: miyazato@kitakyu-u.ac.jp

M. Ezoe
The Kawasaki Heavy Industries, Ltd., 1-1, Kawasaki-cho, Hyogo, Akashi 673-8666, Japan

Published online: 08 February 2022

characteristics and observed the axis-switching phenomenon where the long dimension of the jet column is aligned with the major axis at the nozzle exit and it aligns itself with the minor axis far downstream of the nozzle exit. However, only a qualitative argument was made on the structure of supersonic rectangular jets in almost studies mentioned above and the three-dimensional density field including the near-field shock system in the jet is still not well understood.

It is a challenging issue to capture the three-dimensional structure of non-axisymmetric shock-containing jets. Nonintrusive diagnostics including the laser Doppler velocimetry (LDV), the particle image velocimetry (PIV), and the molecular tagging velocimetry (MTV) are very effective techniques for velocity measurements in internal and external flows. However, the seed particles seem not to follow the sudden change in the velocity fields just behind a strong shock like a Mach stem (Sakurai et al. 2015; Feng and McGuirk 2016; Wernet 2016; Yüceil 2017). These issues lead to inevitable measurement errors. On the other hand, most recently, laser interferometry such as Mach–Zehnder interferometers (Sugawara,Nakao,Miyazato,Ishino and Miki 2020; Kaganovich et al. 2020; Sugawara et al. 2021) and Twyman–Green interferometers (Sugawara,Nakao,Miyazato and Ishino 2018) or schlieren based quantitative optical systems including background oriented schlieren (BOS) (Nicolas et al. 2017; Kaganovich et al. 2020), rainbow schlieren deflectometry (RSD) (Takano et al. 2016; Maeda,Fukuda,Kubo,Nakao,Ono and Miyazato 2018; Mariani et al. 2019, 2020), and calibrated schlieren (Mariani et al. 2019; Nazari et al. 2020) have been utilized to capture the density fields of shock-containing jets. However, their applications have been mostly limited to axisymmetric density fields except for a recent paper of Nazari et al. (2020), who studied systematically the shock-containing jets from circular and square supersonic nozzles. In the present study, the density field of a shock-containing rectangular jet is measured for the first time by the rainbow schlieren deflectometry combined with the computed tomography. The flow topology of the supersonic rectangular jets is examined quantitatively by the visual representation with a high spatial resolution.

2 Experimental apparatus

The experiments were performed in a blowdown compressible air facility of the High-Speed Gasdynamics Laboratory at the University of Kitakyushu. A schematic drawing of the experimental apparatus with the rainbow schlieren optical system is shown in Fig. 1. Ambient air is pressured by the compressor up to 1 MPa and then stored in the high-pressure reservoir consisting of two storage tanks with a total capacity of 2 m^3 after being filtered and dried. The supply line from the reservoir can be connected to the plenum chamber through a coupling, as shown in Fig. 1. Hence, the high-pressure dry air from the reservoir is stagnated in the plenum chamber and then discharged into the atmosphere through a test nozzle. A convergent nozzle with a rectangular cross section of 5mm $\times$ 20mm at the exit was used as the test nozzle. The contour of the short dimension of the nozzle was designed using a sinusoidal curve to provide uniform and parallel flow at the inlet and exit of the nozzle. The nozzle has an inlet height of 30 mm, an exit height of 5 mm, and a constant width of 20 mm over the entire length. The total temperature in the plenum chamber was equal to the room temperature $T_b(= 300.1\text{K} \pm 0.1\text{K})$, and the plenum pressure $p_{os}(= 402\text{kPa} \pm 50\text{Pa})$ was controlled and maintained constant during the testing by a valve, and the back pressure p_b was 100.5 kPa.

The jet issued from the nozzle was visualized by the rainbow schlieren deflectometry for a nozzle pressure ratio of $\text{NPR}(= p_{os}/p_b) = 4.0$. The rainbow schlieren system consists of rail-mounted optical components including a spatial filter with a 50-μm-diameter pinhole, two 100-mm-diameter, 500-mm focal length achromatic lenses, a computer-generated 35-mm-wide rainbow filter with color gradation in a 2.5-mm-wide strip, and a digital camera (Nikon D7100, 6000 $\times$ 4000 square pixel resolution with 14 bit pixel depth) with a 30 mm diameter focusing lens of 600 mm focal length. A continuous 250 W metal halide light source (Sigmakoki IMH-250) connected to a 50 μm diameter fiber optic cable provides the light input at the pinhole through a 16.56 mm focal length objective lens.

The rainbow filter used in the present experiments has continuous hue variation from *Hue* = 0 to 350 deg with a precision error of $\pm$ 2.7 deg in a 2.5-mm-wide strip and was placed at the location of the focal point of the decollimating lens. The characteristics of the rainbow filter were performed by traversing the filter in intervals of 20 μm ($\pm$ 1 μm) at the schlieren cutoff plane before starting experiments. The proper design, generation, and calibration of rainbow filters can be found in Agrawal and Wanstall (2018).

The camera output in the RGB format was digitized by a personal computer with 24 bit color frame grabber. Multiple viewing rainbow schlieren pictures of a shock-containing rectangular jet were taken with an exposure time of 1/400 s and ISO 5000 with continuous schlieren light source over a range of nozzle

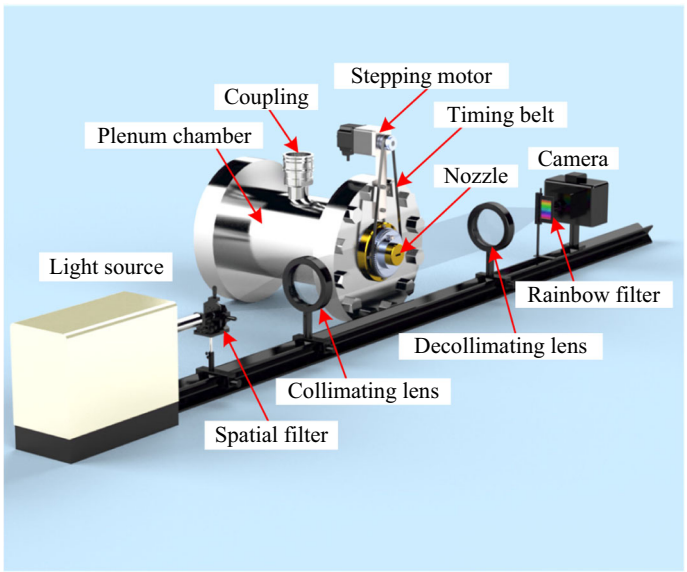

Fig. 1 Experimental setup with rainbow schlieren system

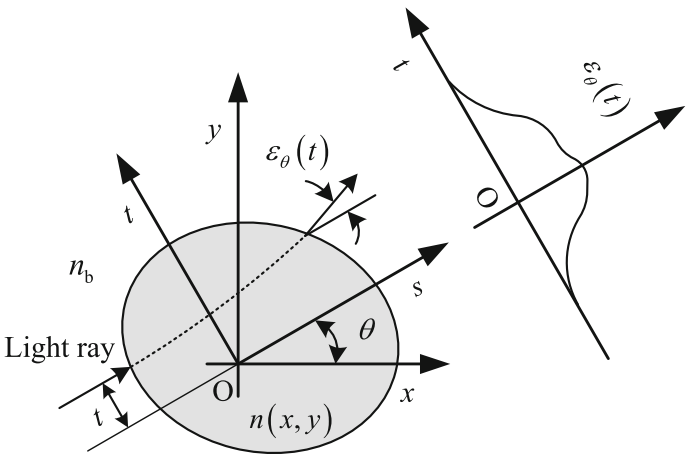

Fig. 2 Light ray traveling through asymmetric refractive index field on jet cross section at fixed streamwise location

angular angles from 0 deg to 180 deg by rotating the nozzle about its longitudinal axis (z axis) in equal angular intervals of 5 deg. The three-dimensional density field of the jet was reconstructed using the convolution back-projection method.

A light ray traveling in a cross section (x, y plane) of an asymmetric jet issued from a nozzle is shown in Fig. 2 where the x, y, z rectangular Cartesian coordinate system is used and the z axis is perpendicular to the x, y plane which includes the vector along the optical axis direction of the schlieren system. Also, the n and n_b in Fig. 2 indicate the refractive index in the jet cross section and that of the surrounding air, respectively. Density fields are investigated for a cross section of z = constant.

As shown in Fig. 2, let us consider the rotated coordinates (s, t) inclined at an angle θ away from the fixed-original coordinates (x, y). Then, a light ray traveling in the s direction with an offset of t from the axis s is bent by the interaction with the jet flow and has an angle of inclination $\varepsilon_\theta(t)$ with respect to its original path. As the incoming ray is initially parallel to the s axis, the deflection angle $\varepsilon_\theta(t)$ after passing through the refractive index field is given by the line integral

$$\varepsilon_\theta(t) = \int_{-\infty}^{\infty} \frac{\partial \eta(s,t)}{\partial t} ds \tag{1}$$

along the s direction of the partial derivative $\partial\eta/\partial t$ with respect to the t variable of the normalized refractive index difference

$$\eta(s,t) \equiv \frac{n - n_b}{n_b} \tag{2}$$

for small ray deflections. The deflection angle $\varepsilon_\theta(t)$ is taken for a range of various angles from $\theta = 0$ deg to 180 deg. The task of tomographic reconstruction in the present investigation is to find $\eta(x,y)$ based upon a given knowledge of $\varepsilon_\theta(t)$ and then density fields can be obtained through a well-known linear relation between refractive index and density, as described later.

After the one-dimensional Fourier transform of Eq. 1 with respect to the t variable and using the Leibniz rule for differentiation under the integral sign, it reduces to a relation,

$$\int_{-\infty}^{\infty} \varepsilon_\theta(t) \exp(-i2\pi t\zeta) dt = 2\pi i\zeta \int_{-\infty}^{\infty}\int_{-\infty}^{\infty} \eta(s,t) \exp(-i2\pi t\zeta) ds dt \tag{3}$$

The transformation from the (s, t)-coordinate to (x, y)-coordinate for the integral of the right-hand side of Eq. 3 yields the following form with $u = -\zeta \sin\theta$ and $v = \zeta \cos\theta$

$$\int_{-\infty}^{\infty}\int_{-\infty}^{\infty} \eta(s,t) \exp(-i2\pi t\zeta) ds dt = \int_{-\infty}^{\infty}\int_{-\infty}^{\infty} \eta(x,y) \exp[-i2\pi(ux + vy)] dx dy \tag{4}$$

This equation expresses the two-dimensional Fourier transform of $\eta(x,y)$. Hence, the inverse Fourier transform of Eq. 3 using the result of Eq. 4 with the convolution theorem leads to

$$\eta(x,y) = \int_0^{\pi} [\varepsilon_\theta(t) * k(t)]_{t=-x\sin\theta+y\cos\theta} d\theta \tag{5}$$

where $k(t)$ is given by

$$k(t) = \frac{\sin^2(\pi t f_{\max})}{\pi^2 t} \tag{6}$$

with the Nyquist frequency, $f_{\max}$, and the asterisk * denotes the convolution between $\varepsilon_\theta(t)$ and $k(t)$ (Agrawal et al. 1998).

When deflection data are sampled at a spacing of Δt, only frequencies below the Nyquist frequency $f_{\max} = 1/(2\Delta t)$ are adequately sampled. The ray deflection angle $\varepsilon_\theta(t)$ is correlated with the focal length f_d of a decollimating lens and the ray transverse displacement $d_\theta(t)$ at the cut-off plane of the schlieren system and given by

$$\varepsilon_\theta(t) = \frac{d_\theta(t)}{f_d} \tag{7}$$

Combination of the Gladstone-Dale relation between the refractive index $n(x, y)$ and the gas density $\rho(x,y)$ with Eq. 2 leads to

$$\rho(x,y) = \rho_b + \frac{n_a \eta(x,y)}{K} \tag{8}$$

Equation 5 can be estimated by its discrete counterpart as

$$\eta(x,y) = \sum_{i=1}^{I} \frac{\pi}{I-1} \sum_{j=1}^{J} \varepsilon\left(\frac{i\pi}{I-1}, j\Delta t\right) \times k(y\cos\theta - x\sin\theta - j\Delta t)\Delta t \tag{9}$$

for I views of J rays each (Agrawal et al. 1998).

The two-dimensional density fields obtained by Eqs. 7 ~ 9 could be stacked together to form the three dimensional density field $\rho(x,y,z)$ of the jet plume.

3 Results and discussion

The flow structure of an underexpanded sonic jet issued from a rectangular convergent nozzle with an aspect ratio of 4 at the exit is given in Fig. 3 with the flow from left to right in which the view shown in Fig. 3a features the nozzle short dimension with the long dimension being perpendicular to the plane of the schlieren picture and vice versa for Fig. 3b showing the view from the nozzle long dimension. An image of the rainbow filter used in the present experiment is depicted at the top of Fig. 3 where the dashed line shows the location of the background hue.

Figure 3a displays distinctive jet boundaries, expansion waves originating from the nozzle lip, and a Mach shock with a short Mach stem located in the first shock cell, which is responsible for the static pressure mismatch at the nozzle exit, but are gradually blurred toward downstream due to the time-dependent unstable movement in the direction normal to the jet centerline (Kaji and Nishimura 1996). Figure 3b shows a Mach shock with a long Mach stem within the first shock cell in which the Mach shock bifurcates into a leading oblique shock and a rear oblique shock with the three intersecting at the bifurcation point, and a similar Mach shock can be dimly observed in the second shock cell. It should be noted that many researchers often compare simulated schlieren images directly to those obtained from experiments with the same flow conditions in order to validate the simulated results in which almost all the verification is performed with a comparison between geometrical shapes such as the angle and length of shocks. However, the verification is meaningful only if the simulated results are spatially averaged along the view direction or if the comparison is performed between vector or scalar quantities at a fixed surface in the flow field.

The density profile along the jet centerline and those along liplines at the major and minor axis planes are shown in Fig. 4 where the profiles are represented with uncertainty errors.

The theoretical density value estimated based upon the assumption of the one-dimensional isentropic flow from the inlet of the nozzle to the exit is shown with a leftward arrow on the vertical axis in Fig. 4a. In addition, the fully expanded jet density ρ_j is calculated based on the assumption that the flow of the nozzle inlet is expanded isentropically to the back pressure, and the resultant density level is shown with the blue solid line parallel to the abscissa. In this regard, it is necessary to keep in mind that the fully expanded jet pressure p_j is identical with the back pressure p_b, but the ρ_j is not equal to the ambient density ρ_b

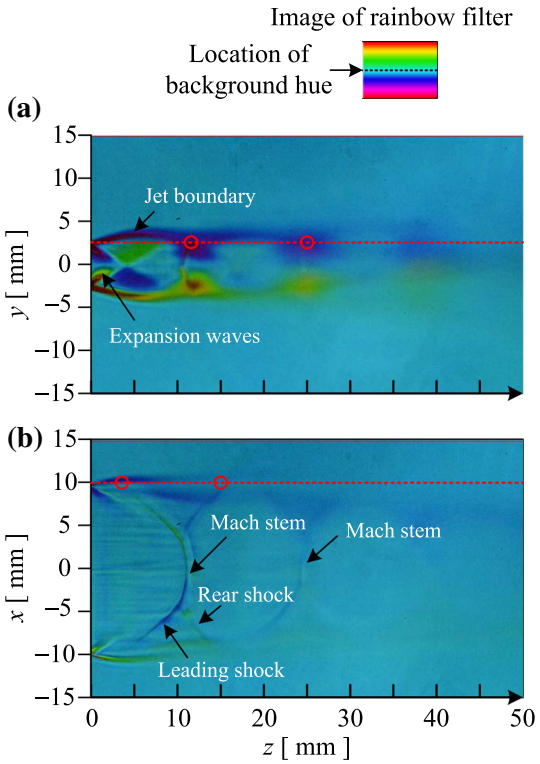

Fig. 3 Rainbow schlieren pictures of shock-containing rectangular jet. **a** minor axis plane view; **b** major axis plane view

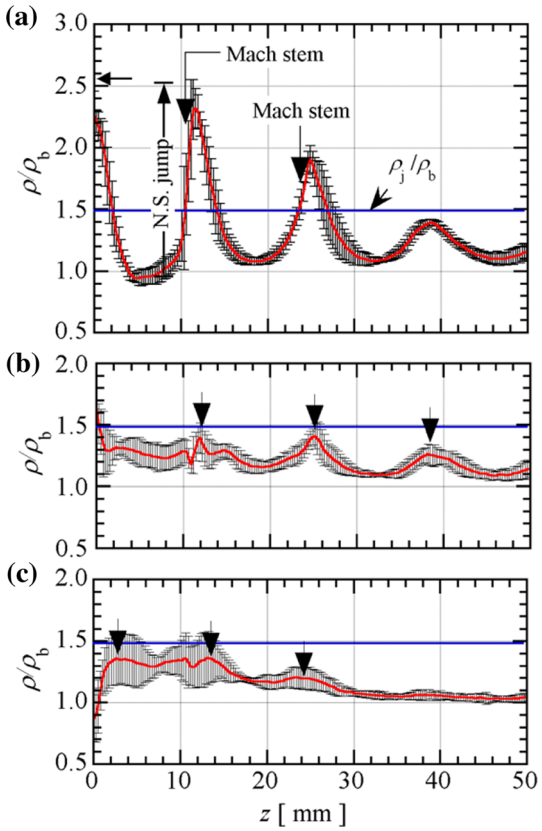

Fig. 4 Streamwise density profiles of **a** jet centerline ($x = y = 0$ mm), **b** lipline at major axis plane ($x = 0$ mm and $y = 2.5$ mm), and **c** lipline at minor axis plane ($x = 10$ mm and $y = 0$ mm)

(Sugawara,Nakao,Miyazato,Ishino and Miki 2020). Since the static pressure at the nozzle exit plane is greater than the back pressure on the present nozzle operating condition (NPR = 4.0 in the present experiment), Prandtl–Meyer expansion waves are produced from the nozzle lip. Therefore, the jet centerline density, as shown in Fig. 4a, also gradually decreases with increasing streamwise distance by the expansion waves until colliding with the Mach stem located at z = around 10 mm, and then rise and fall in density is repeated downstream behind the first Mach stem.

The local maxima in the density profile decrease toward the downstream direction, while the local minima remain almost constant. The density profile across the first Mach stem shows a sudden variation and the density rise across the Mach stem is in good quantitative agreement with the theoretical value estimated using the Rankine–Hugoniot relations. In contrast, the second Mach stem shows the structure with a gradual density variation in the streamwise direction like compression waves. The density profile (Fig. 4b) along the lipline of the minor axis plane exhibits a quasi-periodical wavy form with the three distinctive peaks shown with the downward arrows in which the first peak is caused by the reflection of the rear oblique shock at the jet free boundary, and the other two peaks are also caused by the reflection at the opposite jet boundary of each oblique shock in consecutive downstream shock cells. On the other hand, as shown in Fig. 4c, no distinctive peaks appear on the profile along the lipline of the major axis plane compared with that of the minor axis plane, and the profile remains almost constant over a certain downstream from z = 30 mm in which the shock has no effect on the density profile, but there is a steep rise in the density just after the nozzle exit, which results from the leading oblique shocks originating toward the Mach stem from just downstream of the nozzle lips (x = around 10 mm).

The bird's eye views of the jet density field at the minor and major axis planes on the cross section including the jet centerline are depicted in Fig. 5a and b, respectively, in which the non-dimensional contour levels with an interval of 0.1 are shown at the top of the figure, and the spatial resolution in the density map is around 13 μm. While the schlieren pictures of Figs. 3a and b can provide only integrated information about the density gradient along the direction of the optical axis, Figs. 5a and a can demonstrate clearly the

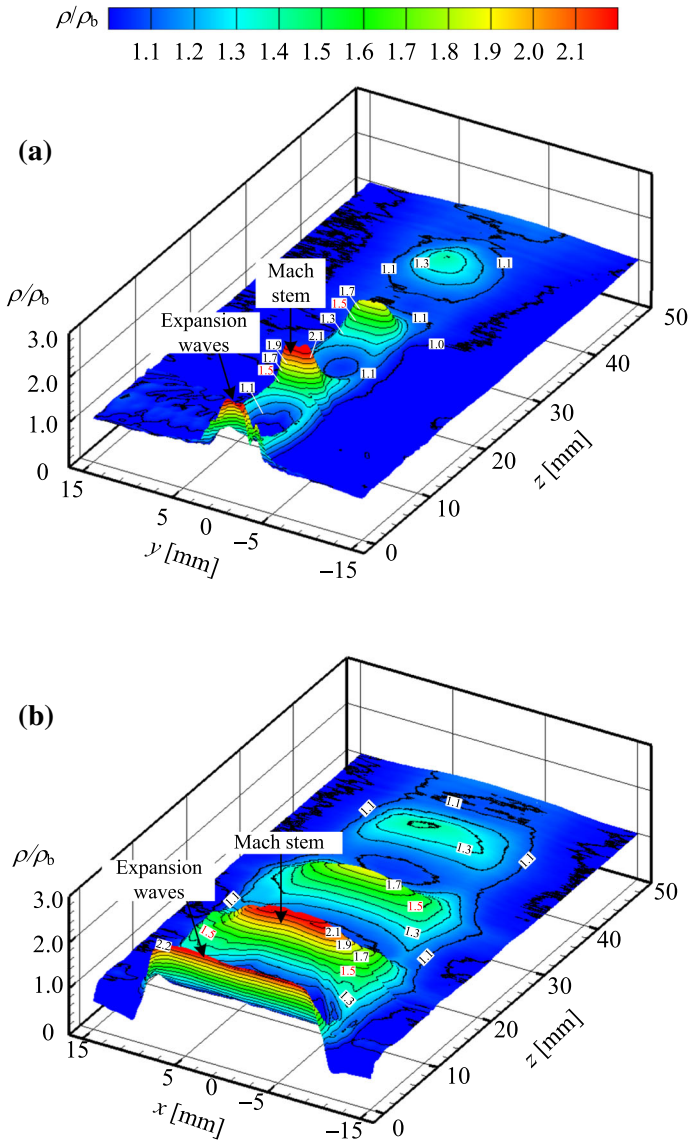

Fig. 5 Bird's eye views for density field of shock-containing rectangular jet. **a** minor axis plane; **b** major axis plane

quantitative information for the spatial variations of the density field of the shock-containing rectangular jet. The downward arrow in each figure shows the position of the Mach stem in the first shock cell on the jet centerline and the values 1.5 shown in red on the density contour map correspond to those at the jet free boundaries (Panda and Seasholtz 1999; Sugawara,Nakao,Miyazato,Ishino and Miki 2020). It should be noted that the densities on the jet free boundaries are higher than the ambient density, although the pressures there coincide with the ambient pressure. Both of the contour maps capture quantitatively the flow topology of an intricate shock-containing rectangular jet including the Mach shock and jet shear layers at a high spatial resolution.

The resolution and sensitivity of the rainbow schlieren system depend primarily on the size of the source aperture, the focal length of the decollimating lens, and the resolution of color gradations on the rainbow filter. A small source aperture, a decollimating lens with longer focal lengths, and a rainbow filter with finer color gradations are desired for superior performance (Agrawal and Wanstall 2018). Hence, the present rainbow schlieren tomography can also be applied for whole field density measurements in microscale non-axisymmetric flows by changing a part of the optical system. More detailed descriptions of the spatial and temporal limitations of rainbow schlieren systems can be found in Al-Ammar et al. (1998), and the application examples of rainbow schlieren techniques are presented by Agrawal and Wanstall (2018).

4 Concluding remarks

The density field of a shock-containing jet issued from a rectangular convergent nozzle with an aspect ratio of 4 at the exit was measured quantitatively for the first time by the rainbow schlieren tomography. The convolution back-projection (CBP) method was utilized to reconstruct the three-dimensional density field. The density profile along the jet centerline and those along the liplines of the minor and major axis planes of the jet were shown to capture the flow feature of the jet. In addition, the flow topology of an intricate near-field shock system in the jet was demonstrated distinctly by the bird's eye view representations on the major and minor axis planes including the jet centerline.

It was found that the rectangular choked jet includes a strong Mach stem in the first shock cell followed by a weak second Mach stem in the second shock cell. The density profile across the first Mach stem exhibits a significant density jump, which is almost the same order of magnitude as the theoretical value by the Rankine–Hugoniot relation, but the second Mach stem has the structure with a gradual density variation like a series of compression waves.

We would like to emphasize that the conventional schlieren pictures can provide only integrated information about the density gradient along the line-of-sight direction, but the rainbow schlieren tomography can demonstrate clearly the quantitative information for the spatial variations of density fields. The rainbow schlieren tomography would be significantly effective to measure the three-dimensional density field of the shock-containing jet issued from a nozzle with any cross section at the exit.

Declarations

Conflict of interest The authors declare that they have no conflict of interest.

References

Agrawal A, Wanstall CT (2018) Rainbow schlieren deflectometry for scalar measurements in fluid flows. J Flow Vis Image Process. https://doi.org/10.1615/JFlowVisImageProc.2018028312

Agrawal AK, Butuk NK, Gollahalli SR, Griffin D (1998) Three-dimensional rainbow schlieren tomography of a temperature field in gas flows. Appl Opt 37(3):479–485

Al-Ammar K, Agrawal AK, Gollahalli SR, Griffin D (1998) Application of rainbow schlieren deflectometry for concentration measurements in an axisymmetric helium jet. Exp Fluids 25(2):89–95

Alkislar MB, Krothapalli A, Lourenco LM (2003) Structure of a screeching rectangular jet: a stereoscopic particle image velocimetry study. J Fluid Mech 489:121

Feng T, McGuirk JJ (2016) Measurements in the annular shear layer of high subsonic and under-expanded round jets. Exp Fluids 57(1):1–25

Gutmark E, Schadow KC, Bicker CJ (1990) Near acoustic field and shock structure of rectangular supersonic jets. AIAA J 28(7):1163–1170

Kaganovich D, Johnson L, Mamonau A, Hafizi B (2020) Benchmarking background oriented schlieren against interferometric measurement using open source tools. Appl Opt 59(30):9553–9557

Kaji S, Nishimura N (1996) Pressure field around a rectangular supersonic jet screech. AIAA J 34(10):1990–1996. https://doi.org/10.2514/3.13344

Krothapalli A, Hsia Y, Baganoff D, Karamcheti K (1986) The role of screech tones in mixing of an underexpanded rectangular jet. J Sound Vib 106(1):119–143

Maeda H, Fukuda H, Kubo K, Nakao S, Ono D, Miyazato Y (2018) Structure of underexpanded supersonic jets from axisymmetric Laval nozzles. J Flow Vis Image Process. https://doi.org/10.1615/JFlowVisImageProc.2018027034

Mariani R, Zang B, Lim H, Vevek US, New TH, Cui Y (2019) A comparative study on the use of calibrated and rainbow schlieren techniques in axisymmetric supersonic jets. Flow Meas Instrum 66:218–228. https://doi.org/10.1016/j.flowmeasinst.2019.01.007

Mariani R, Lim H, Zang B, Vevek U, New T, Cui Y (2020) On the application of non-standard rainbow schlieren technique upon supersonic jets. J Vis 23(3):383–393

Nazari AZ, Ishino Y, Ishiko Y, Ito F, Kondo H, Yamada R, Motohiro T, Miyazato Y, Nakao S (2020) Multi-schlieren CT measurements of supersonic microjets from circular and square micro nozzles. J Flow Control Meas Vis 8(3):77–101

Nicolas F, Donjat D, Léon O, Le Besnerais G, Champagnat F, Micheli F (2017) 3D reconstruction of a compressible flow by synchronized multi-camera BOS. Exp Fluids 58(5):46

Panda J, Seasholtz RG (1999) Measurement of shock structure and shock-vortex interaction in underexpanded jets using Rayleigh scattering. Phys Fluids 11(12):3761–3777. https://doi.org/10.1063/1.870247

Raman G, Rice EJ (1994) Instability modes excited by natural screech tones in a supersonic rectangular jet. Phys of Fluids 6(12):3999–4008

Sakurai T, Handa T, Koike S, Mii K, Nakano A (2015) Study on the particle traceability in transonic and supersonic flows using molecular tagging velocimetry. J Vis 18(3):511–520

Sugawara S, Nakao S, Miyazato Y, Ishino Y (2018) Application of Twyman-Green interferometers for shock-containing free jets from axisymmetric convergent micro nozzles. In: Proceedings 18th International Symposium on Flow Visualization, ETH Zurich

Sugawara S, Nakao S, Miyazato Y, Ishino Y, Miki K (2020) Three-dimensional reconstruction of a microjet with a Mach disk by Mach-Zehnder interferometers. J Fluid Mech. https://doi.org/10.1017/jfm.2020.217

Sugawara S, Nakao S, Miyazato Y, Ishino Y, Miki K (2021) Quantitative flow visualization of slightly underexpanded microjets by Mach-Zehnder interferometers. Flow Turbul Combust 160(3):971–992. https://doi.org/10.1007/s10494-020-00211-4

Takano H, Kamikihara D, Ono D, Nakao S, Yamamoto H, Miyazato Y (2016) Three-dimensional rainbow schlieren measurements in underexpanded sonic jets from axisymmetric convergent nozzles. J Therm Sci 25(1):78–83. https://doi.org/10.1007/s11630-016-0836-0

Wernet MP (2016) Application of tomo-PIV in a large-scale supersonic jet flow facility. Exp Fluids 57(9):1–24

Yüceil KB (2017) A comparison of PIV and interferometric rayleigh scattering measurements in the near field of underexpanded sonic jets. Aerosp Sci Technol 67:31–40